






Efficient and simultaneous capture of iodine and methyl iodide achieved by a covalent organic framework

Yaqiang Xie¹, Tingting Pan¹, Qiong Lei ¹, Cailing Chen¹, Xinglong Dong ¹, Youyou Yuan², Walid Al Maksoud³, Long Zhao⁴, Luigi Cavallo ³, Ingo Pinnau ¹ & Yu Han ^{1,3}✉

Radioactive molecular iodine (I_2) and organic iodides, mainly methyl iodide (CH_3I), coexist in the off-gas stream of nuclear power plants at low concentrations, whereas few adsorbents can effectively adsorb low-concentration I_2 and CH_3I simultaneously. Here we demonstrate that the I_2 adsorption can occur on various adsorptive sites and be promoted through intermolecular interactions. The CH_3I adsorption capacity is positively correlated with the content of strong binding sites but is unrelated to the textural properties of the adsorbent. These insights allow us to design a covalent organic framework to simultaneously capture I_2 and CH_3I at low concentrations. The developed material, COF-TAPT, combines high crystallinity, a large surface area, and abundant nucleophilic groups and exhibits a record-high static CH_3I adsorption capacity ($1.53 \text{ g}\cdot\text{g}^{-1}$ at 25°C). In the dynamic mixed-gas adsorption with 150 ppm of I_2 and 50 ppm of CH_3I , COF-TAPT presents an excellent total iodine capture capacity ($1.51 \text{ g}\cdot\text{g}^{-1}$), surpassing various benchmark adsorbents. This work deepens the understanding of I_2/CH_3I adsorption mechanisms, providing guidance for the development of novel adsorbents for related applications.

¹Advanced Membranes and Porous Materials (AMPM) Center, Physical Science and Engineering Division, King Abdullah University of Science and Technology (KAUST), Thuwal, Saudi Arabia. ²Imaging and Characterization Core Lab, King Abdullah University of Science and Technology (KAUST), Thuwal, Saudi Arabia. ³KAUST Catalysis Center, Physical Science and Engineering Division, King Abdullah University of Science and Technology (KAUST), Thuwal, Saudi Arabia. ⁴State Key Laboratory of Advanced Electromagnetic Engineering and Technology, School of Electrical and Electronic Engineering, Huazhong University of Science and Technology, Wuhan 430074, China. ✉email: yu.han@kaust.edu.sa

Nuclear reactors have been continuously providing ~10% of the world's energy over the last decade¹. As a sustainable and low-carbon energy supply, nuclear energy is expected to play a more important role in the future^{2–4}. However, safety concerns still challenge its operation. One of the major safety issues is the volatile radioactive waste produced during the reprocessing of spent nuclear fuels, which primarily consists of radionuclides, such as ¹²⁹I and ¹³¹I in the form of molecular iodine (I₂) or organic iodides (e.g., methyl iodide (CH₃I) and ethyl iodide)^{4–8}. These compounds are harmful to the environment (¹²⁹I has an extremely long half-life of approximately 1.57 × 10⁷ years) or severely affect human metabolism by damaging the thyroid gland, and must be removed before the off-gas is discharged^{9–11}.

Compared with traditional liquid scrubbing processes to capture radioactive iodine, adsorption-based processes require a simpler operation and lower maintenance costs and avoid highly corrosive solutions⁶. Therefore, researchers have increasingly focused on the development of various adsorbents for iodine capture, including materials containing silver (Ag)^{12–14}, ceramics^{13,15,16}, zeolites^{17,18}, aerogels^{19–21}, metal-organic frameworks^{8,22–26}, and conjugated polymers^{27–31}. Most of these studies have focused on the adsorption capacity of the developed adsorbent for I₂, whereas only a few studies have addressed the capture of CH₃I, and even fewer studies have examined the simultaneous capture of I₂ and CH₃I. Given that radioactive molecular iodine and organic iodides coexist in off-gas streams, it is particularly important to develop adsorbents that can capture them simultaneously and efficiently.

Various strategies have been adopted to promote the adsorption of iodine species. For I₂, effective strategies include the following: (i) using adsorbents containing Ag to precipitate I₂ in the form of silver iodide (AgI)^{2,12,13}, (ii) introducing electron-rich heteroatoms (e.g., nitrogen (N), sulfur (S), and oxygen(O)) or π -donors (e.g., double/triple bonds, benzene rings, and other aromatic compounds) in adsorbents to adsorb electron-deficient I₂ by forming charge-transfer complexes^{32–41}, and (iii) modifying the adsorbent with ionic groups (e.g., [RN-(CH₃)₃]⁺Br[–]) to adsorb I₂ via Coulomb interactions⁴². Compared with I₂, CH₃I is more difficult to capture because of the weaker intermolecular forces⁴³. Currently, the capture of CH₃I is primarily achieved either through catalytic decomposition on adsorbents containing Ag to form AgI^{13,44–46} or through an N-methylation reaction on nucleophilic N sites to form pyridinium³⁴ or quaternary ammonium salts^{1,31,47–49}. Based on these insights, we speculate that adsorbents containing abundant Ag sites or nucleophilic N sites

may exhibit high capture capacity for both I₂ and CH₃I. Given the high cost and poor recyclability of Ag-based adsorbents, developing N-rich adsorbents is a better choice for simultaneously capturing I₂ and CH₃I.

In addition to the characteristics of adsorption sites that determine binding strength, the density of the adsorption sites and the textural properties (e.g., surface area, pore size, and pore volume) of the adsorbent are crucial because these factors collectively determine the number of accessible adsorption sites (i.e., the adsorption capacity) and adsorption kinetics. Therefore, an ideal adsorbent for simultaneously capturing I₂ and CH₃I should possess a high concentration of nucleophilic N sites along with a large surface area and a highly open porous structure.

As an emerging class of porous materials, covalent organic frameworks (COFs) provide an ideal platform for developing high-performance adsorbents because their porous structures and surface functionalities can be easily engineered to meet the requirements of specific applications^{50–52}. Several COFs have been prepared as adsorbents for I₂ capture, in which the binding sites are π -conjugated moieties, various N-containing functional groups, and ionic groups^{34,35,38,42}. Although some of these COFs exhibited high I₂ adsorption capacities in the measurement performed in a static closed system with high partial pressure of I₂, their performance for low-concentration I₂ capture under a dynamic condition was not measured. More importantly, like other recently developed adsorbents, the CH₃I adsorption properties of these COFs have not been investigated.

To the best of our knowledge, there is only one COF material (SCU-COF-2) evaluated for both I₂ and CH₃I adsorption³⁴. In SCU-COF-2, there are pyridine and imine moieties, which bind to I₂ and CH₃I through charge-transfer interaction and N-methylation reactions, respectively. At room temperature, SCU-COF-2 adsorbed 0.979 g g^{–1} I₂ from flowing N₂ (carrier gas) containing 400 ppm of I₂ or 0.564 g g^{–1} of CH₃I from flowing N₂ containing 200,000 ppm of CH₃I. These moderately high adsorption capacities were obtained from single-component measurements, whereas the adsorption performance of SCU-COF-2 in the coexistence of I₂ and CH₃I has not been explored.

In this report, we designed and synthesized two COFs, namely COF-TAPB and COF-TAPT, for the simultaneous capture of I₂ and CH₃I. The framework of COF-TAPB was constructed through imine linkages formed between two monomers, tris(4-formylphenyl)amine (TFPA) and 1,3,5-tris(4-aminophenyl)benzene (TAPB); COF-TAPT is a structural analog of COF-TAPB, constructed from TFPA and 2,4,6-tri(4-aminophenyl)-1,3,5-triazine (TAPT) (see Fig. 1). Through a literature search, we found

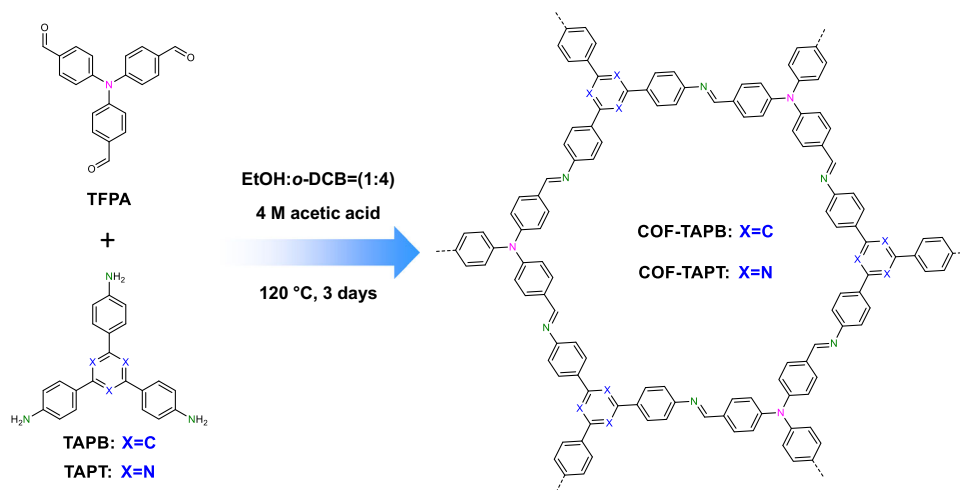


Fig. 1 Schematic illustration of the synthesis of COF-TAPT and COF-TAPB. In the structural model, different N sites are marked with different colors.

that these two COF materials have previously been synthesized for CO₂ adsorption and photocatalytic hydrogen evolution^{53–55}, whereas the synthetic methods are not exactly the same as those used in this study. The two COFs exhibit the same crystal structure and textural properties, being different only in N content, allowing the investigation of the role of N in the adsorption of I₂ and CH₃I.

We evaluated the adsorption properties of the two COFs for I₂ and CH₃I under different conditions (static and dynamic adsorption at different temperatures and adsorbate concentrations) for a direct comparison with benchmark adsorbents reported in the literature. Under the static high-concentration conditions, COF-TAPB and COF-TAPT exhibited similar high I₂ adsorption capacities, and their static I₂ uptake values (7.94 and 8.61 g g⁻¹, respectively) are among the highest reported for various adsorbents. Unlike the case of I₂ adsorption, COF-TAPT exhibited a significantly higher CH₃I uptake capacity than COF-TAPB, suggesting that the N content in the adsorbent plays a vital role in CH₃I adsorption. The further systematic analysis confirmed that the CH₃I adsorption capacity is positively correlated with the N content in the adsorbent. Remarkably, COF-TAPT exhibits a record-high CH₃I adsorption capacity (1.53 g g⁻¹; static conditions at 25 °C), which can be attributed to the combined effect of its high N content (16.1 wt%) and large surface area (~2300 m² g⁻¹). In the dynamic CH₃I adsorption measurement, COF-TAPT demonstrated the highest capacity of all tested adsorbents. When used to simultaneously capture low-concentration I₂ (150 ppm) and CH₃I (50 ppm) from a carrier gas stream, COF-TAPT outperformed all tested adsorbents except an ionic COF in terms of total iodine capture. The adsorbed I₂ and CH₃I can be easily extracted by ethanol or acetone from COF-TAPT to fully restore its adsorption capacity for subsequent adsorption cycles. The density functional theory (DFT) calculations revealed that the CH₃I binding energy at different N sites in COF-TAPT follows the order imine N > triazine N > sp³ N.

Results

Characterization. Powder X-ray diffraction (PXRD) indicated that COF-TAPT and COF-TAPB are highly crystalline, both exhibiting four clearly discernible peaks before 12° (2θ) and two weak peaks at around 16° and 25° (Fig. 2a, c). We performed structural modeling based on PXRD to corroborate that the synthesized COFs have the designed structures. The results revealed that for both materials, the experimental data agree well with the simulated data based on the eclipsed (AA) stacking model (Fig. 2b, d), and the observed diffraction peaks can be indexed as (100), (110), (200), (210), (310), and (001) reflections, respectively. The Pawley fitting results were reasonably good, producing a unit cell of $a = b = 23.51 \text{ \AA}$, $c = 3.64 \text{ \AA}$, $\alpha = \beta = 90^\circ$, and $\gamma = 120^\circ$ ($R_p = 2.15\%$ and $R_{WP} = 2.89\%$) for COF-TAPT (Supplementary Table 1), and a unit cell of $a = b = 23.61 \text{ \AA}$, $c = 3.365 \text{ \AA}$, $\alpha = \beta = 90^\circ$, and $\gamma = 120^\circ$ ($R_p = 2.57\%$ and $R_{WP} = 3.35\%$) for COF-TAPB (Supplementary Table 2). From the N₂ sorption isotherms collected at 77 K (Fig. 2e), the Brunauer–Emmett–Teller (BET) surface areas of COF-TAPT and COF-TAPB are derived at 2348 and 2290 m² g⁻¹, respectively. Their pore size distribution is centered at 1.92 nm (Fig. 2e), which is consistent with the designed structure and PXRD results. The two COFs exhibit very similar PXRD patterns and N₂ adsorption isotherms, indicating that they have comparable structural and textural properties (Supplementary Table 3). High-resolution transmission electron microscopy confirmed that they both possess a hexagonal structure containing one-dimensional channels (Supplementary Fig. 1).

The completion of the Schiff base reaction between TFPA and TAPT/TAPB was evidenced by the disappearances of bands at

3359 to 3428 cm⁻¹ (amino groups) and 1685 cm⁻¹ (aldehyde groups) and the synchronous appearance of the characteristic -C=N- stretching band at ~1625 cm⁻¹ in the Fourier transform infrared (FTIR) spectra (Fig. 2f). The successful construction of the designed COF frameworks and the presence of different N species in the frameworks were further confirmed by solid-state ¹³C nuclear magnetic resonance (NMR) spectroscopy and N 1s X-ray photoelectron spectroscopy (XPS) (Supplementary Fig. 2). In addition, the elemental analysis revealed that the carbon (C), hydrogen (H), and N content in COF-TAPT and COF-TAPB closely agreed with the theoretical values (Supplementary Table 4). These COFs retained high crystallinity after treatment with concentrated HNO₃ aqueous solution (5 M) or β-irradiation (200 kGy), exhibiting the excellent stability required to capture radioactive iodine from the off-gas stream (Supplementary Fig. 3).

Static I₂ and CH₃I adsorption. In most previous studies, I₂ adsorption was performed in a static closed system with saturated I₂ vapor at 75 °C, and the adsorption capacity was determined based on the mass increase subsequently measured under ambient conditions at room temperature^{29,32,33,35–37,56}. To directly compare with the previously developed adsorbents, we evaluated COF-TAPB and COF-TAPT using the same experimental setup (see the Experimental section in the Supporting Information for detailed methods). The results revealed that COF-TAPB and COF-TAPT adsorbed 7.94 and 8.61 g g⁻¹ I₂ within 96 h, respectively (Fig. 3a and Supplementary Table 3). These values rank high among all adsorbents tested under the same conditions (Fig. 3c and Supplementary Table 5). It is worth noting that under this commonly used evaluation condition, where the concentration of I₂ is rather high (~16,000 ppm), the adsorption is dominated by the intermolecular interactions of I₂; consequently, the capacity is largely determined by the pore volume of the adsorbent in addition to the characteristics of the binding sites.

We used the average adsorption rate determined at 80% of the full adsorption capacity ($K_{80\%}$)³⁸ to describe the adsorption kinetics of the adsorbents. Despite their similar porous structures, COF-TAPT exhibited a higher $K_{80\%}$ value than COF-TAPB (0.48 vs. 0.33 g g⁻¹ h⁻¹), which can be attributed to its higher N content promoting the initial adsorption of I₂. The measured I₂ adsorption kinetics of COF-TAPT and COF-TAPB are faster than those of many previously reported microporous adsorbents (Supplementary Table 5) due to their highly crystalline structures that facilitate mass transport. To investigate the effect of porosity on the adsorption capacity and adsorption kinetics, we prepared a control sample, which was synthesized using the same process as COF-TAPT, except that *N,N*-dimethylformamide (DMF) instead of mixed ethanol and *o*-dichlorobenzene was used as the solvent. The obtained material (denoted as TFPA-TAPT) has the same chemical composition as COF-TAPT but a much lower porosity (BET specific surface area: 1284 m² g⁻¹; total pore volume: 0.19 cm³ g⁻¹) due to its poor crystallinity (Fig. 4a, b). Under the same conditions, TFPA-TAPT exhibited a lower I₂ adsorption capacity (4.31 g g⁻¹) and a slower adsorption rate ($K_{80\%}$: 0.098 g g⁻¹ h⁻¹) than COF-TAPT (Supplementary Fig. 4c). This result demonstrates the significant influence of textural properties of the adsorbent on its I₂ adsorption behavior.

We also evaluated the CH₃I adsorption performance of COF-TAPT and COF-TAPB in a static closed system with a saturated CH₃I vapor at 75 °C, as used in the previous study³⁴, for direct comparison. The results demonstrated that COF-TAPT adsorbed 1.53 g g⁻¹ of CH₃I (Fig. 3b), exceeding the capacity of the state-of-the-art CH₃I adsorbent SCU-COF-2 (1.45 g g⁻¹)³⁴. In contrast, COF-TAPB adsorbed only 0.81 g g⁻¹ of CH₃I under the same

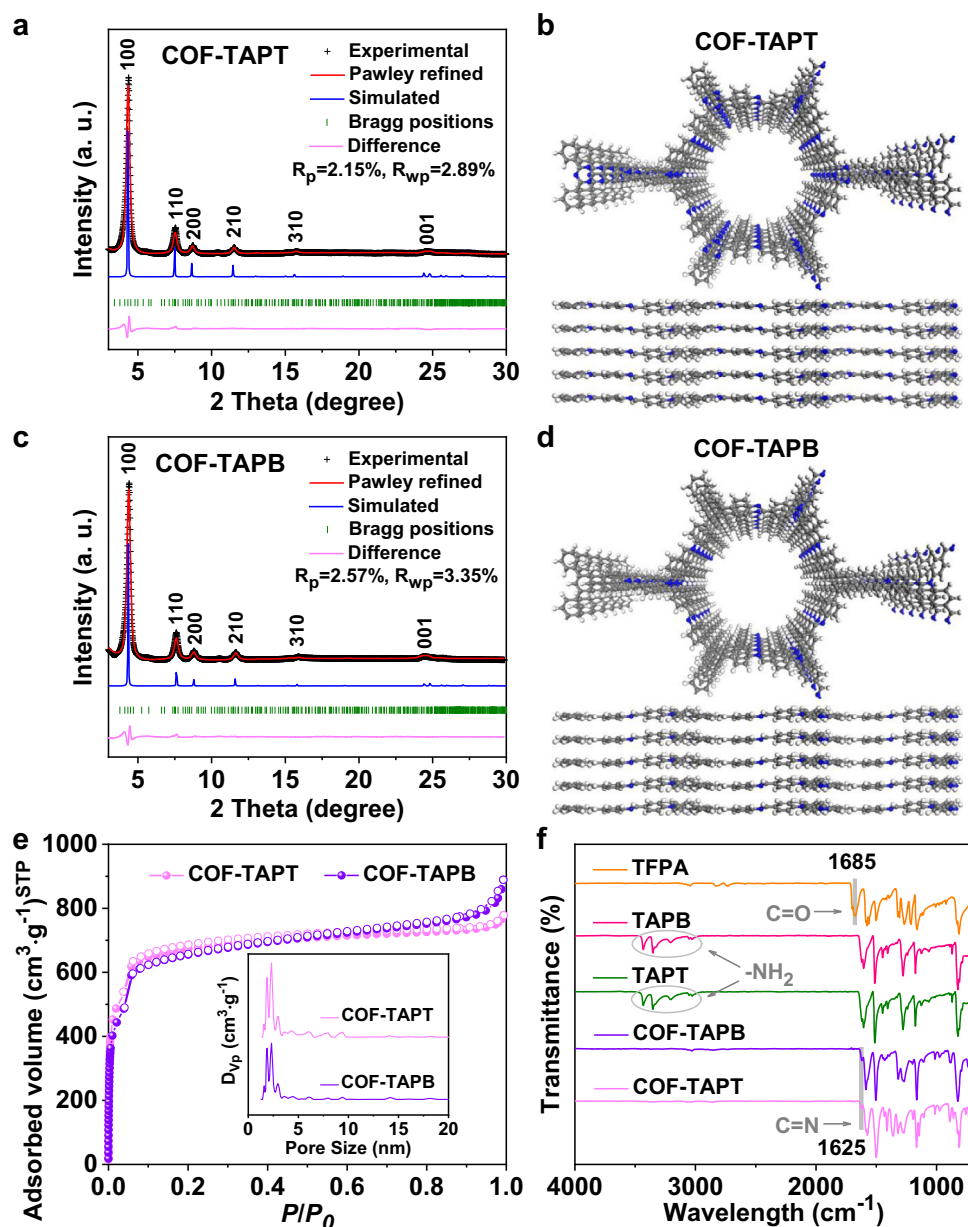


Fig. 2 Structural characterization of COF-TAPT and COF-TAPB. **a, c** PXRD patterns of **a** COF-TAPT and **c** COF-TAPB, with the experimental profiles in black, Pawley refined profiles in red, calculated (from the refined structure model) profiles in blue, and differences between experimental and refined PXRD patterns in pink. Green lines indicate Bragg positions. **b, d** Refined structure model of **b** COF-TAPT and **d** COF-TAPB viewed along the *c*-axis (upper) and *a*-axis (lower). **e** N_2 sorption isotherms of COF-TAPT and COF-TAPB. Inset shows the derived pore size distribution profiles of COF-TAPT and COF-TAPB. **f** FTIR spectra of the synthetic precursors (TFPA, TAPB, and TAPT) and the two COFs (COF-TAPB and COF-TAPT).

conditions (Fig. 3b). The control sample TFPA-TAPT exhibited a CH_3I adsorption capacity of 1.37 g g^{-1} , although its BET surface area is only half of that of COF-TAPT (Supplementary Fig. 4d). These results collectively indicate that, unlike I_2 adsorption, CH_3I adsorption capacity depends on the number of strong binding sites of the adsorbent rather than its surface area or pore volume. This conclusion was further verified by the plots of CH_3I uptake vs. the BET surface area (Supplementary Fig. 5a) and CH_3I uptake vs. N content (Supplementary Fig. 5b), based on the data for seven adsorbents, which clearly indicate that the CH_3I uptake is irrelevant to the surface area but positively correlated with the N content of the adsorbent (Supplementary Table 3). In addition, at their full adsorption capacity, the CH_3I/N ratios in COF-TAPT and COF-TAPB were 0.97 and 0.89, respectively, whereas the I_2/N molar ratios were 3.05 and 4.89, respectively.

These results collectively indicate the essential difference between I_2 adsorption and CH_3I adsorption. The nearly one-to-one correspondence between CH_3I and N suggests that CH_3I molecules are only adsorbed on N sites, presumably by forming salts. In contrast, I_2 adsorption can occur at other sites in the π -conjugated frameworks (e.g., benzene rings) or be promoted by forming polyiodide species, resulting in high I_2/N ratios.

Dynamic I_2 and CH_3I adsorption. Given the low concentrations of molecular iodine and organic iodides (usually <200 ppm) in the off-gas stream^{2,57,58}, it is more meaningful to test the adsorption behavior of adsorbents at low I_2 (or CH_3I) concentrations related to practical applications. To explore the potential of the developed COFs for practical applications, we evaluated their I_2 and CH_3I adsorption capacities under dynamic

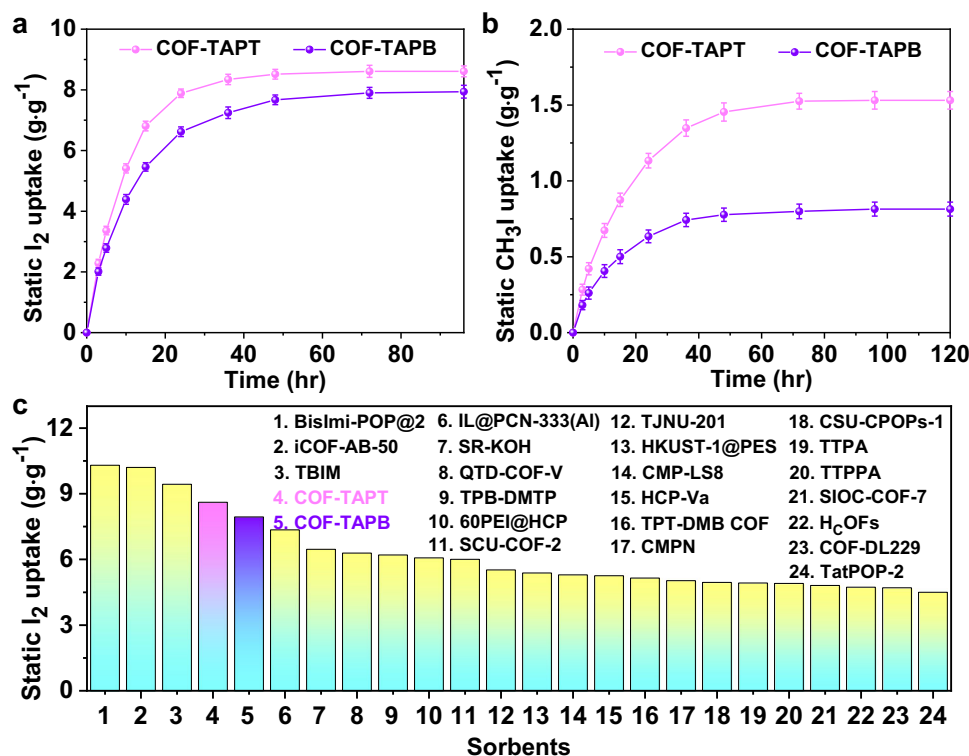


Fig. 3 Static I₂ and CH₃I adsorption performance. Gravimetric measurement of static **a** I₂ and **b** CH₃I vapor adsorption capacities of COF-TAPT and COF-TAPB materials as a function of time at 75 °C. **c** Comparison of the static I₂ adsorption capacities of various high-performance adsorbents. The specific I₂ uptake values of the reported adsorbents and corresponding references are presented in Supplementary Table 5. The error bars are the standard deviations from three parallel measurements.

conditions using a fixed-bed column-breakthrough configuration, which allowed the concentration of I₂ and CH₃I, the temperature of the adsorbent bed, and humidity to be freely adjusted⁴².

To directly compare the developed COFs with benchmark adsorbents^{17,34,42}, we conducted dynamic adsorption at 25 °C with 400 ppm of I₂ in N₂ flow (adsorbent: 30.0 mg; flow rate: 10.0 mL min⁻¹). Under these conditions, COF-TAPB exhibited a steep breakthrough step after 45 h with a total I₂ uptake of 2.18 g g⁻¹, and COF-TAPT demonstrated a similar breakthrough profile, whereas its breakthrough time was 50 h, corresponding to a total I₂ uptake of 2.38 g g⁻¹ (Fig. 4a). The observed I₂ adsorption capacities are significantly higher than those of most reported adsorbents under similar measurement conditions (Supplementary Fig. 6 and Supplementary Table 6). In addition, the presence of water vapor only caused a slight decrease in the I₂ uptake of COF-TAPT (from 2.38 g g⁻¹ to 2.32 g g⁻¹) and COF-TAPB (from 2.18 to 2.13 g g⁻¹) (Fig. 4b), indicating that they are both tolerant to moisture, which is important for practical applications.

We performed dynamic CH₃I adsorption using the same column-breakthrough setup, with the CH₃I concentration controlled at 200,000 ppm. The results revealed that, under dry conditions, the CH₃I uptakes of COF-TAPB and COF-TAPT were 0.71 and 1.30 g g⁻¹, respectively (Fig. 4c, d). The CH₃I adsorption capacity of COF-TAPT (1.30 g g⁻¹) is higher than that of all reported adsorbents except MIL-101-Cr-HMTA¹ (Supplementary Fig. 7 and Supplementary Table 7). The ultrahigh CH₃I adsorption capacity of MIL-101-Cr-HMTA is attributed to the combination of a large surface area and abundant tertiary amine groups that can strongly and specifically interact with CH₃I. However, MIL-101-Cr-HMTA exhibits a limited adsorption capacity for I₂ (Supplementary Fig. 8 and Supplementary Table 6) due to the lack of effective I₂ binding sites other than tertiary amines. When water

vapor was introduced into the feed stream (relative humidity = 50%), the CH₃I adsorption capacity of COF-TAPT decreased from 1.30 to 1.06 g g⁻¹, indicating competitive adsorption between H₂O and CH₃I. This result is because the adsorption of CH₃I primarily occurs on N sites, which also adsorb H₂O molecules. The dynamic adsorption measurements indicate that COF-TAPT has a similar I₂ uptake capacity but a significantly higher CH₃I uptake capacity than COF-TAPB. This outcome is consistent with the results of the static adsorption experiments and further validates the above conclusion about the difference between I₂ adsorption and CH₃I adsorption.

The adsorbed I₂ and CH₃I in COF-TAPT can be fully extracted by ethanol to regenerate its adsorption capacities. When the I₂-saturated COF-TAPT (I₂@COF-TAPT) or CH₃I-saturated COF-TAPT (CH₃I@COF-TAPT) was immersed in ethanol, the I₂ or CH₃I desorption process proceeded spontaneously and accelerated with the assistance of sonication. As a commonly used method for regenerating adsorbents after I₂ adsorption, extraction with ethanol can also efficiently remove CH₃I from COF-TAPT because the N-methylation reaction is reversible in protic solvents⁵⁹. The regenerated COF-TAPT (COF-TAPT-Re) restored its original physiochemical properties, as evidenced by the FTIR, PXRD, and N₂ sorption characterizations. Correspondingly, the exceptionally high adsorption capacity of COF-TAPT can be fully restored in four successive adsorption/extraction cycles under the above conditions (Supplementary Figs. 9, 10).

Simultaneous capture of low-concentration I₂ and CH₃I. After evaluating the adsorption performance of the developed COFs for I₂ and CH₃I under commonly used conditions, we explored their ability to capture I₂ and CH₃I at much lower concentrations (150 and 50 ppm, respectively) relevant to practical off-gas treatment applications. Several state-of-the-art adsorbents for I₂ or CH₃I

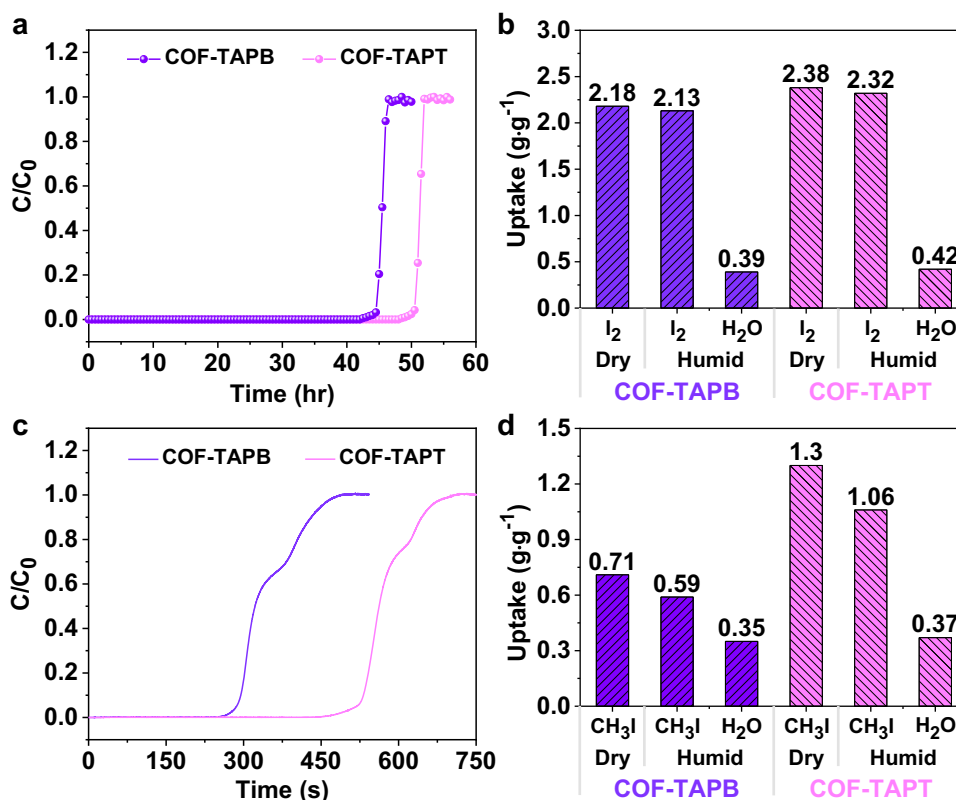


Fig. 4 Dynamic I₂ adsorption and CH₃I adsorption performances. **a** I₂ breakthrough profiles of COF-TAPB and COF-TAPT at 25 °C. The concentration of I₂ in the carrier gas is 400 ppm. **b** Dynamic I₂ uptake values of COF-TAPB and COF-TAPT under dry and humid conditions. The water uptake under humidity is also presented. **c** CH₃I breakthrough profiles of COF-TAPB and COF-TAPT at 25 °C. The concentration of CH₃I in the carrier gas is 200,000 ppm. **d** Dynamic CH₃I uptake values of COF-TAPB and COF-TAPT under dry and humid conditions. The water uptake under humidity is also presented.

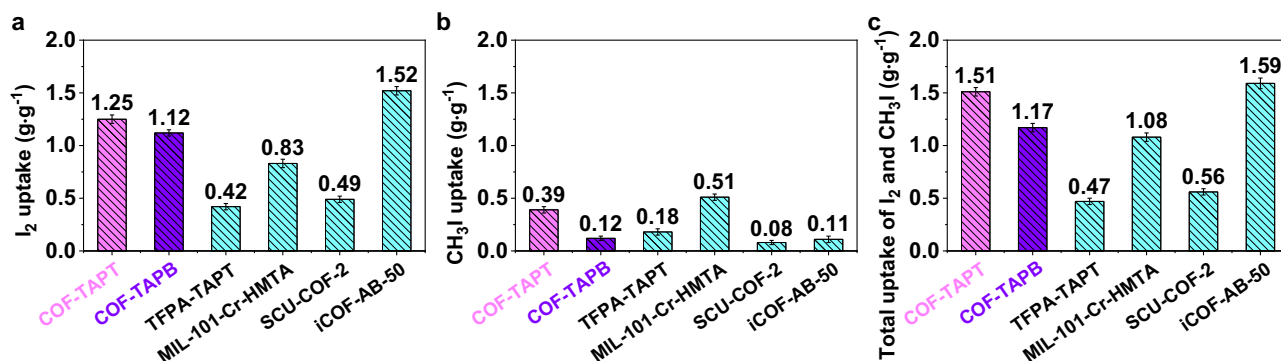


Fig. 5 Comparison of different adsorbents in dynamic adsorption capacity. The capacities were measured from **a** single-component I₂ at 150 ppm, **b** single-component CH₃I at 50 ppm, **c** mixed-component (150 ppm I₂ and 50 ppm CH₃I) breakthrough experiments performed at 25 °C. The error bars are the standard deviations from three parallel measurements.

capture, including MIL-101-Cr-HMTA¹, SCU-COF-2³⁴, and iCOF-AB-50⁴², were evaluated under the same conditions for comparison. We started with single-component measurements, introducing only I₂ (150 ppm) or CH₃I (50 ppm) in the feed stream for capture. The results revealed that, for I₂ capture, the order of adsorption capacity of the tested adsorbents is iCOF-AB-50 (1.52 g g⁻¹) > COF-TAPT (1.25 g g⁻¹) > COF-TAPB (1.12 g g⁻¹) > MIL-101-Cr-HMTA (0.83 g g⁻¹) > SCU-COF-2 (0.49 g g⁻¹) > TFPA-TAPT (0.42 g g⁻¹) (Fig. 5a and Supplementary Table 8). This order is consistent with that derived from the static adsorption measurements (Fig. 3c). The exceptionally high I₂ uptake of iCOF-AB-50 is attributed to the presence of abundant ionic groups that

effectively promote I₂ adsorption via strong Coulomb interactions. The results of various adsorbents capturing CH₃I, as summarized in Fig. 5b and Supplementary Table 8, indicate that COF-TAPT ranks second among all tested adsorbents. The specific CH₃I adsorption capacities are as follows: MIL-101-Cr-HMTA (0.51 g g⁻¹) > COF-TAPT (0.39 g g⁻¹) > TFPA-TAPT (0.18 g g⁻¹) > COF-TAPB ≈ iCOF-AB-50 (0.12 g g⁻¹) > SCU-COF-2 (0.08 g g⁻¹).

These results further confirm that the adsorption behaviors of I₂ and CH₃I are different. The adsorption of I₂ can be initiated through specific functional groups (e.g., ionic groups) in the adsorbent and further promoted through strong intermolecular interactions. Therefore, the type of binding sites and textural

properties of the adsorbent both critically influence the I₂ uptake. In contrast, the adsorption of CH₃I is primarily determined by the type and number of binding sites and is not much related to the textural properties of the adsorbent. In addition, ionic groups can strongly promote the adsorption of I₂ but have a little promotional effect on the adsorption of CH₃I because I₂ can be easily induced to form charge species, such as I₃⁻ and I₅⁻, whereas CH₃I cannot.

Finally, we measured the simultaneous capture of iodine species on various adsorbents by co-feeding I₂ (150 ppm) and CH₃I (50 ppm). Considering the excellent capture ability of COF-TAPT for I₂ and CH₃I in the single-component measurements, good performance in the co-capture of these two species is expected. Indeed, COF-TAPT exhibited a significantly higher total iodine (I₂ + CH₃I) capture capacity (1.51 g g⁻¹) than other tested adsorbents, except iCOF-AB-50 (Fig. 5c and Supplementary Table 8). The total uptake of iCOF-AB-50 primarily derives from the contribution of I₂ adsorption; thus, it is conceivable that COF-TAPT is more suitable for feed streams containing a high fraction of organic iodide. Similar to the single-component measurement results, the high performance of the COF-TAPT in simultaneous capture of I₂ and CH₃I can be fully regenerated in successive tests (Supplementary Fig. 11).

Discussion

To analyze the adsorption sites of COF-TAPT, we characterized the I₂-saturated COF-TAPT sample (I₂@COF-TAPT) with PXRD after the static adsorption measurement. The obtained PXRD pattern did not exhibit diffraction peaks related to the original crystalline structure of COF-TAPT (Supplementary Fig. 9b), indicating the loss of structural order due to the incorporation of I₂ into the porous channels. Moreover, no diffraction peaks associated with I₂ were observed, ruling out the possibility that the high I₂ adsorption capacity of COF-TAPT was caused by the recrystallization of I₂ outside its porous structure. Solid-state ¹³C NMR spectra revealed that the chemical shifts of all carbon atoms in COF-TAPT changed to a certain extent after the adsorption of I₂ (Fig. 6a), suggesting that I₂ molecules interacted with various sites throughout the entire π -electron conjugated framework^{27,34}. The N 1s XPS indicated that after the adsorption of I₂, the peak fractions at 398.6 and 399.5 eV, assigned to imine/triazine N and sp³ N in COF-TAPT^{33,34}, shifted to 400.7 and 401.4 eV, respectively (Fig. 6b), suggesting the formation of charge-transfer complexes between I₂ and various N species in COF-TAPT. In the FTIR spectra, the adsorption of I₂ caused the bands of C=N at 1625 cm⁻¹, C=C at 1586 cm⁻¹, C-N (in N-ph₃) at 1361 cm⁻¹, and C-N (in ph-N=C) at 1195 cm⁻¹ to decrease in intensity or shift (Fig. 6c), indicating that all functional groups in the entire framework of COF-TAPT interact with I₂^{27,33,34}. The Raman spectrum of I₂@COF-TAPT exhibited characteristic bands at 107.5, 142.2, and 166.7 cm⁻¹, which can be assigned to the symmetric stretching vibration of I₃⁻, asymmetric stretching vibration of I₃⁻, and stretching vibration of I₅⁻, respectively (Fig. 6d)^{60,61}. These spectroscopic observations indicate that various functional groups in COF-TAPT, including phenyl rings, imine and triazine moieties, and sp³ N, were all involved in forming the charge-transfer complex with I₂ and that polyiodide species were produced during the adsorption process.

The CH₃I-saturated COF-TAPT sample (CH₃I@COF-TAPT) was also characterized using ¹³C NMR, N 1s XPS, and FTIR. Compared to the original material, CH₃I@COF-TAPT exhibited an intense new signal at ~58.9 ppm in the ¹³C NMR spectrum, originating from CH₃I that formed salts at various N sites

through methylation reactions (Fig. 6a)³⁴. In addition, after the adsorption of CH₃I, the N 1s electron binding energies of imine/triazine N and sp³ N in COF-TAPT increased by 1.3 and 3.7 eV, respectively, providing additional evidence for the binding of CH₃I on N species (Fig. 6b)^{1,34}. Compared with I₂ adsorption, CH₃I adsorption resulted in a less pronounced peak shift for imine/triazine N and a more pronounced peak shift for sp³ N, implying differences in affinity of I₂ and CH₃I at different N sites. In FTIR, the adsorption of CH₃I on COF-TAPT also resulted in the intensity change or shift of the characteristic bands of C=N and C-N bonds, and the appearance of a band at ~939 cm⁻¹ indicated the formation of new C-N bonds on the heterocycles in COF-TAPT (Fig. 6c)^{31,34}. Notably, the bands of C=C at 1560–1590 cm⁻¹ were unchanged upon the adsorption of CH₃I. These spectroscopic results support the conclusion that CH₃I molecules are not adsorbed on the benzene ring moieties in COF-TAPT but are specifically bonded to the nucleophilic N sites through N-methylation reactions. The CH₃I-adsorbed COF-TAPT exhibits strong anion-exchange ability (Supplementary Fig. 12), confirming the generation of exchangeable iodide ions.

There are three types of nucleophilic N species (i.e., imine, triazine, and sp³ N) in COF-TAPT, all of which can bind to CH₃I. To gain more insight into the preferential binding sites of CH₃I, we performed DFT calculations to assess their binding energies with CH₃I. The calculations were conducted at the B3LYP^{62,63} level of the exchange functional, using TFPA-T as the model molecule to represent COF-TAPT (Fig. 7). The calculated binding energy is -15.0 kcal mol⁻¹ for imine, -5.4 kcal mol⁻¹ for triazine, and -2.6 kcal mol⁻¹ for sp³ N sites, indicating that the imine groups in the COF are the most favorable adsorption sites for CH₃I (Fig. 7). This result suggests that introducing imine groups and maximizing their content in the adsorbent may be a good choice to improve the ability to capture low-concentration CH₃I. In previous studies, sp³ N promoted the capture of CH₃I, where N was connected with alkyl chains^{1,47,48}. However, in TFPA-T, sp³ N is connected with three benzene rings; thus, its nucleophilicity is greatly reduced due to the conjugation effect. We note that the XPS data (Fig. 6b) suggest that CH₃I interacts more strongly with sp³ N than with imine/triazine N (more pronounced peak shift). This discrepancy is not fully understood and requires further exploration.

In conclusion, the development of high-performance adsorbents for the simultaneous capture of molecular iodine and organic iodides relies on understanding the similarities and differences between these two processes. Based on previous studies, we hypothesized that N-rich carbonaceous adsorbents are conducive to simultaneously capturing I₂ and CH₃I. Further studies revealed that I₂ could be relatively easily adsorbed on a variety of electron-donor sites, including various N species and aromatic moieties, by forming charge-transfer complexes and polyiodides. Therefore, the characteristics of binding sites and textural properties (e.g., surface area and pore volume) of the adsorbent both affect I₂ uptake. The adsorption of CH₃I occurs specifically on nucleophilic N sites through N-methylation reactions to form salts and is unrelated to the textural properties of the adsorbent. In addition, ionic groups can strongly promote the adsorption of I₂ but have little promotional effect on the adsorption of CH₃I. These findings motivated the development of a COF-based adsorbent, COF-TAPT, which combines a high surface area and numerous nucleophilic N sites, including imine, triazine, and sp³ N, thereby exhibiting excellent adsorption capacity for I₂ and CH₃I. We evaluated COF-TAPT for I₂ and CH₃I adsorption under different conditions and found that it outperforms most state-of-the-art adsorbents in all measurements, especially at low-concentration conditions relevant to practical applications. In addition, we calculated the binding energies of CH₃I at different

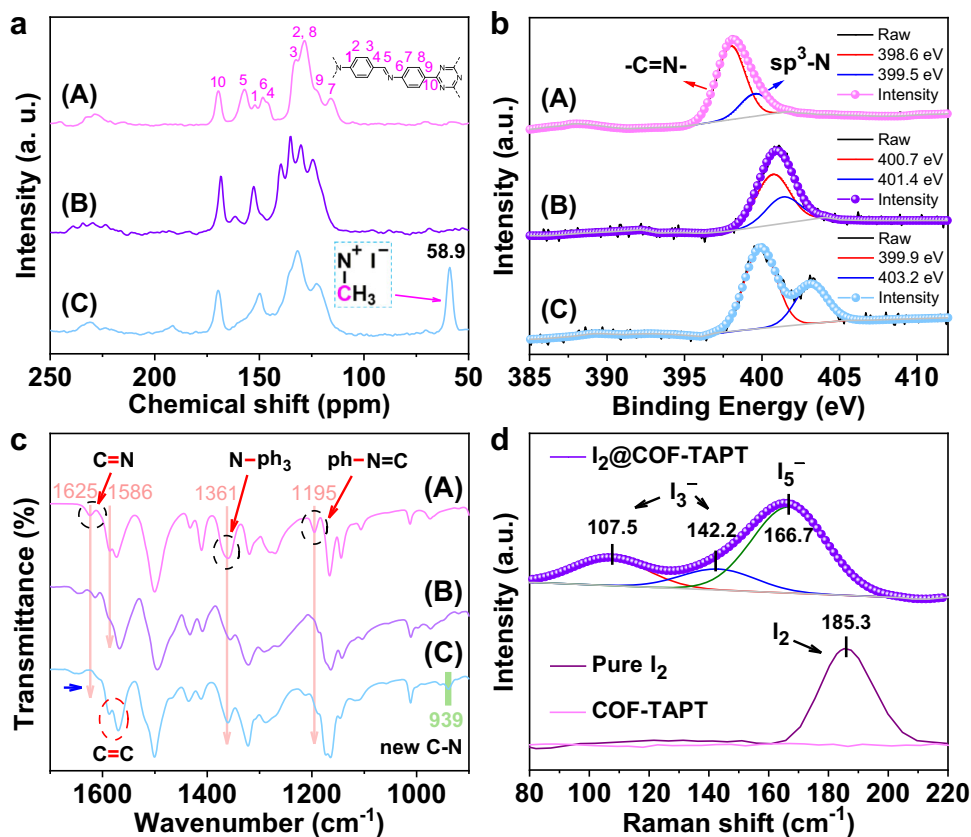


Fig. 6 Characterization of I_2 /adsorbent and CH_3I /adsorbent interactions. **a** ^{13}C NMR spectra of (A) pristine, (B) I_2 -saturated, and (C) CH_3I -saturated COF-TAPT. **b** N 1s XPS spectra of (A) pristine, (B) I_2 -saturated, and (C) CH_3I -saturated COF-TAPT. **c** FTIR spectra of (A) pristine, (B) I_2 -saturated, and (C) CH_3I -saturated COF-TAPT. **d** Raman spectra of pure I_2 , pristine COF-TAPT, and I_2 -saturated COF-TAPT.

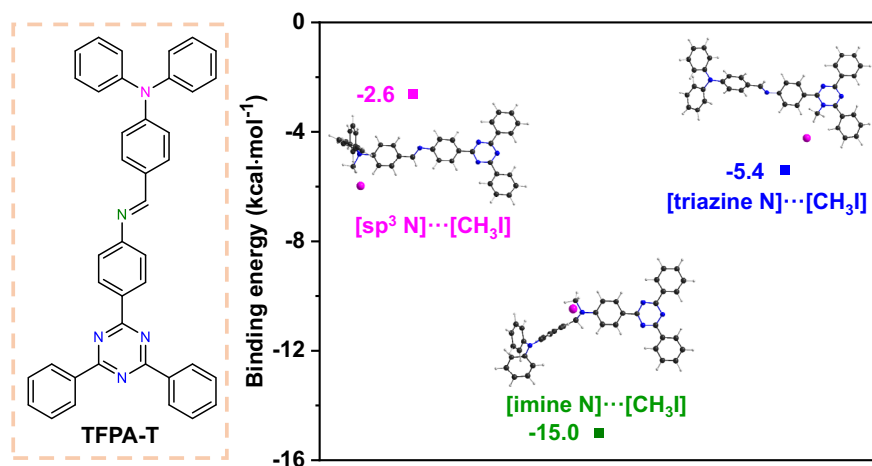


Fig. 7 Density functional theory calculations of the binding energies of CH_3I with different N sites. TFPA-T is the model molecule used for calculations that represent COF-TAPT. In the molecular structure of TFPA-T (left panel), sp^3 N, imine N, and triazine N are labeled in pink, green, and blue, respectively.

N sites, and the results revealed that imine groups might be the most preferred adsorption sites.

Received: 18 December 2021; Accepted: 11 May 2022;
Published online: 24 May 2022

Data availability

All data supporting the findings of this study are available within the article and the Supplementary information file, or available from the corresponding authors on request.

References

- Li, B. et al. Capture of organic iodides from nuclear waste by metal-organic framework-based molecular traps. *Nat. Commun.* **8**, 485 (2017).

- Riley, B. J., Vienna, J. D., Strachan, D. M., McCloy, J. S. & Jerden, J. L. Jr Materials and processes for the effective capture and immobilization of radioiodine: a review. *J. Nucl. Mater.* **470**, 307–326 (2016).
- Huve, J. et al. Porous sorbents for the capture of radioactive iodine compounds: a review. *RSC Adv.* **8**, 29248–29273 (2018).
- Xie, W., Cui, D., Zhang, S.-R., Xu, Y.-H. & Jiang, D.-L. Iodine capture in porous organic polymers and metal–organic frameworks materials. *Mater. Horiz.* **6**, 1571–1595 (2019).
- Svensson, P. H. & Kloo, L. Synthesis, structure, and bonding in polyiodide and metal iodide–iodine systems. *Chem. Rev.* **103**, 1649–1684 (2003).
- Nandanwar, S. U., Coldsnow, K., Utgikar, V., Sabharwal, P. & Aston, D. E. Capture of harmful radioactive contaminants from off-gas stream using porous solid sorbents for clean environment—A review. *Chem. Eng. J.* **306**, 369–381 (2016).
- Taghipour, F. & Evans, G. J. Radiolytic organic iodide formation under nuclear reactor accident conditions. *Environ. Sci. Technol.* **34**, 3012–3017 (2000).
- Chebbi, M., Azambre, B., Volkringer, C. & Loiseau, T. Dynamic sorption properties of Metal-Organic Frameworks for the capture of methyl iodide. *Microporous Mesoporous Mater.* **259**, 244–254 (2018).
- Taylor, D. M. The radiotoxicology of iodine. *J. Radioanalytical Chem.* **65**, 195–208 (1981).
- Goldsmith, J. R. et al. Juvenile hypothyroidism among two populations exposed to radioiodine. *Environ. Health Perspect.* **107**, 303–308 (1999).
- Michel, R. et al. Iodine-129 in soils from Northern Ukraine and the retrospective dosimetry of the iodine-131 exposure after the Chernobyl accident. *Sci. Total Environ.* **340**, 35–55 (2005).
- Munakata, K., Kanjo, S., Yamatsuki, S., Koga, A. & Ianovski, D. Adsorption of noble gases on silver-mordenite. *J. Nucl. Sci. Technol.* **40**, 695–697 (2003).
- Chapman, K. W., Chupas, P. J. & Nenoff, T. M. Radioactive iodine capture in silver-containing mordenites through nanoscale silver iodide formation. *J. Am. Chem. Soc.* **132**, 8897–8899 (2010).
- Tang, S., Choi, S., Nan, Y. & Tavlarides, L. L. Adsorption of methyl iodide on reduced silver-functionalized silica aerogel: kinetics and modeling. *AIChE J.* **67**, e17137 (2021).
- Wilkinson, M., Mondino, A. & Manzini, A. Separation of iodine produced from fission using silver-coated alumina. *J. Radioanalytical Nucl. Chem.* **256**, 413–415 (2003).
- Riley, B. J., Chong, S., Olszta, M. J. & Peterson, J. A. Evaluation of getter metals in Na–Al–Si–O aerogels and xerogels for the capture of iodine gas. *ACS Appl. Mater. Interfaces* **12**, 19682–19692 (2020).
- Pham, T. C. T. et al. Capture of iodine and organic iodides using silica zeolites and the semiconductor behaviour of iodine in a silica zeolite. *Energy Environ. Sci.* **9**, 1050–1062 (2016).
- Park, S., An, H., Park, M. B. & Lee, J. Adsorption behavior of methyl iodide on a silver ion-exchanged ZSM-5. *Microporous Mesoporous Mater.* **294**, 109842–109847 (2020).
- Riley, B. J. et al. Chalcogen-based aerogels as sorbents for radionuclide remediation. *Environ. Sci. Technol.* **47**, 7540–7547 (2013).
- Riley, B. J. et al. Polyacrylonitrile-chalcogel hybrid sorbents for radioiodine capture. *Environ. Sci. Technol.* **48**, 5832–5839 (2014).
- Subrahmanyam, K. S. et al. Chalcogenide aerogels as sorbents for radioactive iodine. *Chem. Mater.* **27**, 2619–2626 (2015).
- Chapman, K. W., Sava, D. F., Halder, G. J., Chupas, P. J. & Nenoff, T. M. Trapping guests within a nanoporous metal–organic framework through pressure-induced amorphization. *J. Am. Chem. Soc.* **133**, 18583–18585 (2011).
- Bennett, T. D., Saines, P. J., Keen, D. A., Tan, J. C. & Cheatham, A. K. Ball-milling-induced amorphization of zeolitic imidazolate frameworks (ZIFs) for the irreversible trapping of iodine. *Chem. A Eur. J.* **19**, 7049–7055 (2013).
- Hughes, J. T., Sava, D. F., Nenoff, T. M. & Navrotsky, A. Thermochemical evidence for strong iodine chemisorption by ZIF-8. *J. Am. Chem. Soc.* **135**, 16256–16259 (2013).
- Valizadeh, B., Nguyen, T. N., Smit, B. & Stylianou, K. C. Porous metal-organic framework@polymer beads for iodine capture and recovery using a gas-sparged column. *Adv. Funct. Mater.* **28**, 1801596 (2018).
- Lei, Y. et al. Visualization of gaseous iodine adsorption on single zeolitic imidazolate framework-90 particles. *Nat. Commun.* **12**, 4483 (2021).
- Yan, Z., Yuan, Y., Tian, Y., Zhang, D. & Zhu, G. Highly efficient enrichment of volatile iodine by charged porous aromatic frameworks with three sorption sites. *Angew. Chem. Int. Ed.* **54**, 12733–12737 (2015).
- Liao, Y., Weber, J., Mills, B. M., Ren, Z. & Faul, C. F. Highly efficient and reversible iodine capture in hexaphenylbenzene-based conjugated microporous polymers. *Macromolecules* **49**, 6322–6333 (2016).
- Shetty, D. et al. Lithiated polycalix[4]arenes for efficient adsorption of iodine from solution and vapor phases. *Chem. Mater.* **29**, 8968–8972 (2017).
- Janeta, M., Bury, W. & Szafer, S. Porous silsesquioxane–imine frameworks as highly efficient adsorbents for cooperative iodine capture. *ACS Appl. Mater. Interfaces* **10**, 19964–19973 (2018).
- Jie, K. et al. Mechanochemical synthesis of pillar [5] quinone derived multi-microporous organic polymers for radioactive organic iodide capture and storage. *Nat. Commun.* **11**, 1086 (2020).
- Niu, T.-H., Feng, C.-C., Yao, C., Yang, W.-Y. & Xu, Y.-H. Bisimidazole-based conjugated polymers for excellent iodine capture. *ACS Appl. Polym. Mater.* **3**, 354–361 (2020).
- Xu, M., Wang, T., Zhou, L. & Hua, D. Fluorescent conjugated mesoporous polymers with N, N-diethylpropylamine for the efficient capture and real-time detection of volatile iodine. *J. Mater. Chem. A* **8**, 1966–1974 (2020).
- He, L. et al. A nitrogen-rich covalent organic framework for simultaneous dynamic capture of iodine and methyl iodide. *Chem* **7**, 699–714 (2021).
- Wang, P. et al. Exceptional iodine capture in 2D covalent organic frameworks. *Adv. Mater.* **30**, 1801991 (2018).
- Jiang, X. et al. Topochemical synthesis of single-crystalline hydrogen-bonded cross-linked organic frameworks and their guest-induced elastic expansion. *J. Am. Chem. Soc.* **141**, 10915–10923 (2019).
- Geng, T. et al. Poly {tris [4-(2-thienyl) phenyl] amine} and poly [tris (4-carbazoyl-9-yl phenyl) amine] conjugated microporous polymers as adsorbents for highly efficient iodine adsorption. *J. Solid State Chem.* **265**, 85–91 (2018).
- Guo, X. et al. Colyliform crystalline 2D covalent organic frameworks with quasi-3D topologies for rapid I₂ adsorption. *Angew. Chem. Int. Ed.* **132**, 22886–22894 (2020).
- Geng, T., Zhang, W., Zhu, Z. & Kai, X. Triazine-based conjugated microporous polymers constructing triphenylamine and its derivatives with nitrogen as core for iodine adsorption and fluorescence sensing I₂. *Microporous Mesoporous Mater.* **273**, 163–170 (2019).
- Xiong, S. et al. Carbazole-bearing porous organic polymers with a mulberry-like morphology for efficient iodine capture. *ACS Appl. Mater. Interfaces* **11**, 27335–27342 (2019).
- Geng, T., Zhang, C., Liu, M., Hu, C. & Chen, G. Preparation of biimidazole-based porous organic polymers for ultrahigh iodine capture and formation of liquid complexes with iodide/polyiodide ions. *J. Mater. Chem. A* **8**, 2820–2826 (2020).
- Xie, Y. et al. Ionic functionalization of multivariate covalent organic frameworks to achieve an exceptionally high iodine-capture capacity. *Angew. Chem. Int. Ed.* **60**, 22432–22440 (2021).
- Bruffey, S. H., Jubin, R. T. & Jordan, J. *Organic Iodine Adsorption by AgZ Under Prototypical Vessel Off-Gas Conditions*. Report No. ORNL/TM-2016/568, (United States: N. P., 2016).
- Jubin, R. *Organic Iodine Removal from Simulated Dissolver Off-Gas Systems Utilizing Silver-Exchanged Mordenite*. Report No. CONF-811108--14. (Oak Ridge National Lab, 1981).
- Funabashi, K., Fukasawa, T. & Kikuchi, M. Investigation of silver-impregnated alumina for removal of radioactive methyl iodide. *Nucl. Technol.* **109**, 366–372 (1995).
- Nenoff, T. M., Rodriguez, M. A., Soelberg, N. R. & Chapman, K. W. Silver-mordenite for radiologic gas capture from complex streams: dual catalytic CH₃I decomposition and I confinement. *Microporous Mesoporous Mater.* **200**, 297–303 (2014).
- Park, S. W., Park, H. S., Lee, W. K. & Moon, H. Effect of water vapor on adsorption of methyl iodide to triethylenediamine-impregnated activated carbons. *Sep. Technol.* **5**, 35–44 (1995).
- González-García, C., González, J. & Román, S. Removal efficiency of radioactive methyl iodide on TEDA-impregnated activated carbons. *Fuel Process. Technol.* **92**, 247–252 (2011).
- Wang, J., Fan, D., Jiang, C. & Lu, L. Host-guest interaction-mediated nanointerface engineering for radioiodine capture. *Nano Today* **36**, 101034 (2021).
- Feng, X., Ding, X. & Jiang, D. Covalent organic frameworks. *Chem. Soc. Rev.* **41**, 6010–6022 (2012).
- Ding, S.-Y. & Wang, W. Covalent organic frameworks (COFs). From design to applications. *Chem. Soc. Rev.* **42**, 548–568 (2013).
- Geng, K. et al. Covalent organic frameworks: design, synthesis, and functions. *Chem. Rev.* **120**, 8814–8933 (2020).
- Zhai, L., Huang, N., Xu, H., Chen, Q. & Jiang, D. A backbone design principle for covalent organic frameworks: the impact of weakly interacting units on CO₂ adsorption. *Chem. Commun.* **53**, 4242–4245 (2017).
- Puthiraj, P., Kim, H. S., Yu, K. & Ahn, W.-S. Triphenylamine-based covalent imine framework for CO₂ capture and catalytic conversion into cyclic carbonates. *Microporous Mesoporous Mater.* **297**, 110011 (2020).
- Yang, J. et al. Protonated imine-linked covalent organic frameworks for photocatalytic hydrogen evolution. *Angew. Chem. Int. Ed.* **60**, 19797–19803 (2021).

56. Tang, Y., Huang, H., Li, J., Xue, W. & Zhong, C. IL-induced formation of dynamic complex iodide anions in IL@MOF composites for efficient iodine capture. *J. Mater. Chem. A* **7**, 18324–18329 (2019).
57. Burger, L. L. & Scheele, R. D. *HWVP Iodine Trap Evaluation* (Pacific Northwest National Lab, 2004).
58. Jubin, R. T., Soelberg, N. R., Strachan, D. M. & Ilas, G. *Fuel Age Impacts on Gaseous Fission Product Capture During Separations*. Report No. PNNL-22550, (Pacific Northwest National Lab, 2012).
59. Katritzky, A. R., Meth-Cohn, O. & Rees, C. W. *Comprehensive Organic Functional Group Transformations: Synthesis: Carbon with One Heteroatom Attached by a Single Bond* (Elsevier, 1995).
60. Hsu, S., Signorelli, A., Pez, G. & Baughman, R. Highly conducting iodine derivatives of polyacetylene: Raman, XPS and x-ray diffraction studies. *J. Chem. Phys.* **69**, 106–111 (1978).
61. Cambedouzou, J. et al. Raman spectroscopy of iodine-doped double-walled carbon nanotubes. *Phys. Rev. B* **69**, 235422–235427 (2004).
62. Kim, K. & Jordan, K. Comparison of density functional and MP2 calculations on the water monomer and dimer. *J. Phys. Chem.* **98**, 10089–10094 (1994).
63. Stephens, P. J., Devlin, F. J., Chabalowski, C. F. & Frisch, M. J. Ab initio calculation of vibrational absorption and circular dichroism spectra using density functional force fields. *J. Phys. Chem.* **98**, 11623–11627 (1994).

Acknowledgements

This research is supported by the AMPM CCF fund (FCC/1/1972-43-01) to Y.H. from King Abdullah University of Science and Technology.

Author contributions

Y.X. and Y.H. conceived the project and designed the experiments. Y.X. and W.A.M. prepared and characterized the materials. Y.X., T.P., and X.D. conducted the adsorption experiments. C.C. performed TEM measurement and analysis. Y.X. and Y.Y. performed PXRD simulations and analysis. L.Z. helped the irradiation treatments. L.C. performed the DFT calculations. Y.X., Q.L., I.P., and Y.H. wrote the manuscript with contributions from all the authors.

Competing interests

The authors declare no competing interests.

Additional information

Supplementary information The online version contains supplementary material available at <https://doi.org/10.1038/s41467-022-30663-3>.

Correspondence and requests for materials should be addressed to Yu Han.

Peer review information *Nature Communications* thanks Feng Luo, Shuao Wang and the other, anonymous, reviewer(s) for their contribution to the peer review of this work. Peer reviewer reports are available.

Reprints and permission information is available at <http://www.nature.com/reprints>

Publisher's note Springer Nature remains neutral with regard to jurisdictional claims in published maps and institutional affiliations.



Open Access This article is licensed under a Creative Commons Attribution 4.0 International License, which permits use, sharing, adaptation, distribution and reproduction in any medium or format, as long as you give appropriate credit to the original author(s) and the source, provide a link to the Creative Commons license, and indicate if changes were made. The images or other third party material in this article are included in the article's Creative Commons license, unless indicated otherwise in a credit line to the material. If material is not included in the article's Creative Commons license and your intended use is not permitted by statutory regulation or exceeds the permitted use, you will need to obtain permission directly from the copyright holder. To view a copy of this license, visit <http://creativecommons.org/licenses/by/4.0/>.

© The Author(s) 2022